HHS Public Access

Author manuscript

Nat Cell Biol. Author manuscript; available in PMC 2013 February 01.

Published in final edited form as:

Nat Cell Biol. 2012 August ; 14(8): 838–849. doi:10.1038/ncb2541.

Synaptotagmin-Like Proteins Control Formation of a Single Apical Membrane Domain in Epithelial Cells

Manuel Gálvez-Santisteban[1,*], **Alejo E. Rodriguez-Fraticelli**[1,*], **David M. Bryant**[2], **Silvia Vergarajauregui**[1,§], **Takao Yasuda**[5], **Inmaculada Bañón-Rodríguez**[1], **Ilenia Bernascone**[1], **Anirban Datta**[2], **Natalie Spivak**[2,3], **Kitty Young**[2], **Christiaan L. Slim**[2,‡], **Paul R. Brakeman**[2,3], **Mitsunori Fukuda**[5], **Keith E. Mostov**[2,4], and **Fernando Martín-Belmonte**[1]

[1]Centro de Biología Molecular Severo Ochoa Consejo Superior de Investigaciones Científicas, Madrid 28049, Spain

[2]Department of Anatomy, University of California San Francisco, California 94143-2140, USA

[3]Department of Pediatrics, University of California San Francisco, California 94143-2140, USA

[4]Department of Biochemistry and Biophysics, University of California San Francisco, California 94143-2140, USA

[5]Department of Developmental Biology and Neurosciences, Graduate School of Life Sciences, Tohoku University, Aobayama, Aoba-ku, Sendai, Miyagi 980-8578, Japan

SUMMARY

The formation of epithelial tissues requires both the generation of apical-basal polarity and the co-ordination of this polarity between neighboring cells to form a central lumen. During *de novo* lumen formation, vectorial membrane transport contributes to formation of a singular apical membrane, resulting in contribution of each cell to only a single lumen. Here, from a functional screen for genes required for 3D epithelial architecture we identify key roles for Synaptotagmin-like proteins 2-a and 4-a (Slp2-a/4-a) in generation of a single apical surface per cell. Slp2-a localizes to the luminal membrane in a PI(4,5)P_2-dependent manner, where it targets Rab27-loaded vesicles to initiate a single lumen. Vesicle tethering and fusion is controlled by Slp4-a, in conjunction with Rab27/Rab3/Rab8 and the SNARE Syntaxin-3. Together, Slp2-a/4-a co-ordinate the spatiotemporal organization of vectorial apical transport to ensure only a single apical surface, and thus formation of a single lumen, occurs per cell.

Correspondence: Fernando Martín-Belmonte, CBMSO, CSIC-UAM, C/Nicolás Cabrera 1, 28049 Madrid, Tel: 34-911964615, Fax: 34-911964420, fmartin@cbm.uam.es.

§Present Address: National Heart, Lung and Blood Institute (NHLBI), National Institute of health (NIH) Bethesda, MD 20824-0105, USA.

‡Present Address: Dept. Cell Biology, University Medical Center Groningen, Antonius Deusinglaan 1, Groningen 9713 AV, Holland

*These authors contributed equally to this work

The authors declare that they have no competing financial interests

AUTHOR CONTRIBUTIONS

M.G.S, A.E.R.F, D.M.B., S.V. and , F.M.-B. designed the experiments. M.G.S, A.E.R.F, D.M.B., S.V, T.S., I.B.R:, I.B., A.D., N.S., K.Y., and C.L.S. did the experimental work. M.G.S, A.E.R.F, D.M.B. K.E.M., and F.M.-B. analysed the experiments. P.R.B and M.F. provided reagents. F.M.-B., D.M.B. M.G.S, and A.E.R.F wrote the manuscript.

Keywords

Cell polarity; epithelial morphogenesis; Rab GTPases; phosphoinositides; vesicle trafficking; lumen formation; synaptotagmin-like proteins

INTRODUCTION

Epithelia represent the most fundamental tissue in metazoa, forming complex layers of cells such as the skin, or kidney tubules. The epithelial plasma membrane is divided into two domains: apical and basolateral, separated by cellular junctions, dependent on the asymmetric delivery and segregation of membrane proteins and lipids[1,2]. Such plasma membrane asymmetry allows the formation of a central lumen, and hence the evolution of specialized functions for different metazoan tissues[3]. Epithelial cells create lumens via an array of morphogenetic mechanisms. Despite this diversity, a series of common molecular events create biological tubes: vectorial transport to a nascent apical domain, *de novo* apical plasma membrane biogenesis, and secretion and expansion of the luminal space[4,5]. Transport of apical proteins to the initial site for apical-membrane formation, at which the Par3–aPKC–Cdc42 polarity complex is established, is controlled by a Rab11a/8a GTPase cascade and its effectors, the exocyst and Myo5B[6,7]. At the lumen, phosphoinositide asymmetry is concomitantly established with $PI(4,5)P_2$ and $PI(3,4,5)P_3$ localizing to, and specifying, the apical and basolateral domains, respectively[8,9]. How vectorial exocytic transport is coordinated and directed so that each cell has a single apical initiation site, and thus the tube has a single lumen, however, is largely unclear. Similarly, how such machineries are controlled at the transcriptional level during morphogenesis of epithelial tissues is poorly understood[3].

Here, we report a functional screen for regulators of 3-dimensional (3D) epithelial polarity using MDCK cyst cultures, based on transcriptional, RNAi, and morphogenetic analysis.

Synaptotagmin-like proteins (Slp1–5) are a family of Rab effectors involved in regulated exocytosis[10]. Slps harbour a N-terminal Rab-binding domain (also called Slp-homology-domain SHD), and tandem C-terminal C2 domains involved in Ca^{2+} and phospholipid binding, and function in tethering secretory vesicles to the plasma membrane[11]. In *D. melanogaster*, a single divergent Slp paralogue, Bitesize (Btsz), functions in epithelial polarization[12], though whether mammalian Slps function in polarity generation is unknown.

We demonstrate that Slp2-a and related family member Slp4-a function in distinct, but complimentary, steps of apical transport to form a lumen *de novo*. Slp2-a controls positioning of Slp4-a/Rab27-positive vesicles to target exocytosis to a single $PI(4,5)P_2$-enriched lumen. Slp4-a regulates the tethering of these vesicles, through the association with the apical SNARE Syntaxin-3, to mediate vesicle delivery to the lumen. Thus, through a functional, multi-step screen we have identified a previously uncharacterized mechanism for co-ordianated vectorial transport, crucial to form a single apical domain.

RESULTS

Identification of 14 previously uncharacterized regulators of epithelial morphogenesis

We performed a multi-step, functional screen for regulators specifically of 3D epithelial architecture and morphogenesis. We first conducted a microarray-based differential expression analysis comparing the transcriptome of MDCK cells undergoing apical-basolateral polarization either in traditional monolayer culture ('2D'), or as 3D cysts grown in basement membrane extract ('3D'), wherein MDCK self-assemble to form a 3D monolayer (Figure 1A). Notable transcriptional differences were observed during 3D morphogenesis with 1597 upregulated, and 1304 downregulated probes detected (Figure S1). To prioritize functional analyses, upregulated genes were subjected to bioinformatic analysis to reconstruct potential molecular pathways and known components of epithelial polarization. Using this approach, a set of 99 upregulated genes was selected for secondary validation by qPCR (Figure S2, Table S1). Finally, 47 candidate genes were targeted via siRNA, including the known polarity regulators Claudin-2 (CLDN2) and Wrch-1 (RHOU) as internal controls[13,14](Figure 1B; Table S2). We found a set of 14 genes previously uncharacterized to be required for this process (Figure 1B–C, green stars; Table S3). These included tight and adherens junctions, Rho GTPases, lipid signaling, and membrane trafficking proteins.

To analyze a possible relevance of these genes *in vivo*, we analyzed whether this gene set was downregulated in human cancers, suggesting an importance in the maintenance of a differentiated epithelial phenotype *in vivo* (Figure 1D). Notably, renal, breast, and skin cancers presented with the strongest downregulation of this gene set. We selected one of these genes, SYTL2 (Slp2-a), which was significantly downregulated in several epithelial cancer datasets (Figure 1E), to characterize its role in lumen formation.

Slp2-a associates with, and regulates formation of, the luminal membrane

The mammalian Slp family has been shown to regulate primarily Rab27-dependent membrane trafficking and secretion[15–17], but their function in mammalian epithelial morphogenesis is unknown. We confirmed that Slp2-a protein levels were upregulated in 3D compared to 2D cultures (14-fold enrichment at 72h; Figure 2A), and qPCR data (Figure S2). Next, we characterized Slp2-a localization in MDCK cysts. Upon plating MDCK into 3D, the apical Podocalyxin (Podxl) localized to the peripheral surface of early aggregates, before it is internalized into vesicles and delivered to the contact between two cells, where lumen is formed *de novo*[7,9,18]. In early aggregates, Slp2-a localized to the plasma membrane, enriched at cellular junctions (Figure 2B, Table 1). A pool of Slp2-a became apparent on internalized Podxl-positive transcytosing vesicles near the cell-cell contact (Figure 2B, 16–20h). Upon lumen formation (24–48h), Slp2-a localized to the apical membrane (Figure 2B, 48h).

Slp2-a depletion perturbed 3D lumen formation in a dose-dependent manner (Figure 2C–E), without affecting cell polarity in cells growing in monolayers (Figure S3A). Slp2-a depletion results in abnormal morphology with multiple small lumens (Figure 2D), and the accumulation of Podxl (Figure 2D), that we identify as transcytotic vesicles (Figure S5C).

Notably, stable expression of RNAi-resistant human Slp2-a (Slp2-aGFP; Figure 2F) completely rescued lumen formation and morphogenesis of cysts with endogenous Slp2-a KD (Figure 2G,H). Moreover, these results indicate that Slp2-a is the predominant variant required for epithelial morphogenesis in 3D-MDCK[19].

The SHD and C2 domains play non-redundant roles in targeting Slp2-a to membranes

Slp-family proteins share an amino-terminal Rab27-binding domain (the 'Slp-homology domain', SHD), a linker region, and two c-terminal tandem C2-domains (phospholipid and/or protein interaction sites)[20,21]. Slp2-a could potentially therefore connect Rab-GTPases and phosphoinositides during lumen formation[9,22,23]. To elucidate the control of Slp2-a localization, we analyzed Slp2-a domains during cyst formation. In early aggregates, the C2-domains localized to the plasma membrane and to cell-cell junctions, but not to Podxl-vesicles (Figure 3A, S4B, 12–20h). Once lumens formed, C2A/B fragment localized exclusively to the apical membrane (Figure 3A, S4B, 24–48h). In contrast, the SHD fragment was predominantly cytoplasmic, and partially localized to Podxl-vesicles in early aggregates and subapically in mature cysts (Figure 3A, bottom panels). Deletion of the C2 domains (GFP–ΔC2A/B) resulted in a similar localization to the SHD, while linker region was cytoplasmic (Figure S4). These results suggest that while the SHD binds to apical vesicles, the C2-domains target Slp2-a to membranes.

Notably, the distribution of the C2-domains resembles $PI(4,5)P_2$ localization during cyst formation[9]. Furthermore, Slp2-a, and paralogues, bind selectively to $PI(4,5)P_2$[12,17], although it could bind also to phosphatidyl-serine (PS)[16]. We found that C2-domains bound specifically to PIP_2 species, but not to PS (Figure 3C). Furthermore, Lact-C2-GFP, a probe for PS, presents non-polarized membrane localization in cysts (Figure S4E). Given the established role of $PI(4,5)P_2$ in apical membrane specification[9], and higher cellular abundance[24], we reasoned that $PI(4,5)P_2$ may target Slp2-a to plasma membranes. During cyst formation Slp2-a and $PI(4,5)P_2$ co-localized at the plasma membrane, becoming progressively enriched to the lumen in morphogenesis (Figure 3D). Furthermore, both $PI(4,5)P_2$ and Cherry-Slp2-a disappeared rapidly from the apical membranes upon Ionomycin treatment, which causes membrane PIP-depletion[25] (Figure 3E, Video S1). Taken together, these results confirm that Slp2-a requires the C2 domains for $PI(4,5)P_2$ binding and apical membrane localization, whereas the SHD region targets Slp2-a to apically destined vesicles (Figure 3F).

Slp2-a targets Rab27 vesicles to the lumen initiation site to form the lumen

Nearly all described functions of mammalian Slps required the SHD domain[21]. In contrast, *bitesize*, the sole Slp paralogue in Drosophila does not require a Rab-binding domain for epithelial morphogenesis[12] (Figure S5B), suggesting Rab-Slp interactions may be dispensable for epithelial polarity. To address this possibility, we expressed the epithelial *bitesize* protein (Btsz2-GFP) and an SHD-deleted Slp2-a mutant (GFP-Slp2-a-ΔSHD). Importantly, neither GFP-Slp2-a-ΔSHD nor *Btsz2-GFP* was able to rescue the defects caused by endogenous Slp2-a KD (Figure 4A–C, Figure S4B). These results reveal that the SHD region is required for epithelial morphogenesis in MDCK cysts.

To determine which Rab-GTPase interactions are required for Slp2-a function we analyzed Rabs that interact with other Slps[10]. Slp2-a bound to Rab3b, Rab8a, Rab27a, and to a lower extent Rab3a (Figure S5A). While Rab8a/b are required for cyst formation[7,18], only KD of both Rab27a/b strongly perturbed lumen formation (Figure 4D–G), confirming partial isoform redundancy noted from knockout mice[26]. In contrast, while Rab3a-d isoforms are expressed in MDCK (data not shown), silencing of Rab3b was sufficient to disrupt cyst formation (Figure 4D–G), suggesting Rab3b may have subtle non-redundant roles in apical transport[27,28], and epithelial polarity. These results suggested that Slp2-a could mediate the targeting of apical vesicles loaded with Rab27a/b, Rab3b and/or Rab8a/b.

Next, we generated Slp2-a-SHD mutants to disrupt interaction with specific Rabs based on structure of the Slp2-a/Rab27 interaction[20]. Introduction of a V18A mutation in Slp2-a completely abolished interaction with Rab3b and Rab8a, while preserving Rab27a binding; E11A/R32A mutations also disrupted the binding to Rab27 (Figure 4G). Although both mutants retain apical localization (Figure 4I, Table 1), GFP-Slp2-a-V18A, but not E11A/R32A, completely rescued the Slp2-a KD phenotype (Figure 4H–I, Figure S5F). Together, these data indicate that although Slp2-a can bind multiple Rabs, Rab27a/b is necessary and sufficient for Slp2-a function in lumen morphogenesis.

Next, we analyzed Rab27 localization. Before lumen formation, GFP-Rab27a colocalized with Podxl and Slp2-a in vesicles transcytosing to the lumen (Figure 4J, top and middle panels; Figure S5C). Once lumen initiation was completed, Rab27a localized to a subapical compartment, while Slp2-a localized apically (Figure 4J, bottom panels; Figure S5C–E). Finally, Slp2-a KD caused the scattering of Rab27a vesicles close to the plasma membrane (Figure 4K, bottom panels). Thus, Slp2-a is required to localize Rab27a. Taken together, these results indicate that Slp2-a binds to Rab27a-loaded apical vesicles and targets them to initiate the lumen.

Slp4-a additionally functions in lumen biogenesis

In addition to Slp2-a, mammalian cells express four additional Slp-family proteins (Slp1–5), and 4 closely related Slac2s (Slp homologue lacking C2 domains)[10]. To determine whether additional Slps proteins function in epithelial polarization, we analyzed their expression during lumen formation. Notably, while Slp2-a was the sole Slp upregulated in 3D at early times (Figure 5A, 3D-14h), Slp1 and Slp4-a were upregulated at later times (Figure 5A, 3D-36h).

In contrast to Slp1, Slp4-a silenced cysts presented acute defects with formation of multiple lumens and internal vesicles (Figure 5B–C). In addition, Slp4-a KD did not affect polarity or ciliogenesis in monolayers (Figure S3A–B). Moreover, we observed Slp2-a is specifically induced before Slp4-a in 3D cultures (Figure 5D), suggesting Slp2-a is required earlier than Slp4 in lumenogenesis.

We next examined the localization of Slp4-a. Endogenous Slp4a/b and GFP-Slp4-a associated with apical membranes at all stages of polarization (Figure 5E, S6D), thus presenting a different localization pattern than Slp2-a (see Figure 3, Table 1). Next, we examined Slp4-a domains in cysts. The C2 domains (C2A/B), either alone or in tandem,

localized to apical and basolateral plasma membranes (Figure 5F, left panels; Figure S6E, Table 1), suggesting they confer non-specific plasma membrane localization. In support of this, GST-Slp4-a C2 domains bound promiscuously to $PI(4,5)P_2$ and $PI(3,4,5)P_3$ (Figure 5G–H, S6C). In contrast, the C2A domain of Slp2-a bound specifically to $PI(4,5)P_2$ and localized apically (Figure S4D), suggesting that only Slp2-a is able to tether Rab27 vesicles to apical $PI(4,5)P_2$-enriched plasma membrane. Together, these data highlight a requisite of the SHD-linker region for apical targeting of Slp4-a, representing a major difference with Slp2-a, and suggesting non-redundant roles for Slp2-a and Slp4-a in lumen formation.

Slp4-a apical localization and function depend on Rab and syntaxin interaction

Slp4-a functions in docking of secretory granules with the plasma membrane, a function modulated by the SHD region, which interacts with Rab3, Rab8, and Rab27 family members[10]. Therefore, we examined Rab binding contribution to Slp4-a function.

To elucidate the role of Rab binding we examined the ability of SHD mutations to bind to Rab27/3/8 and to rescue the phenotype of endogenous Slp4-a KD (Figure 6A–B)[29]. In contrast to apical WT-Slp4-a, removal of the Rab-interacting region of Slp4-a (ΔSHD) resulted in both cytoplasmic and non-polarized membrane localization of Slp4-a (Figure 6C, Figure S6E, Table 1), similar to W118S-Slp4-a (no-Rab-binding) expression (Figure 6A–C, Figure S6F, Table 1). Uncoupling of Slp4-a from Rab3b (V21A) resulted in subapical localization (Figure 6C, Figure S6F). In contrast, co-uncoupling of Rab8 and Rab3b (I18A) resulted in the targeting of a pool of Slp4-a to the basolateral membrane, in addition to subapical vesicles (Figure 6A–C, Figure S6F, Table 1). While WT-Slp4-a was able to rescue endogenous Slp4-a KD, none of the Rab-binding mutants were able to restore lumen formation (Figure 6B–C, Table 1). These results indicate that Rab27, Rab8 and Rab3 binding are required for Slp4-a localization and function. The different localization of the mutants also suggests that Rab27 is required for Slp4-a targeting to vesicles, Rab8 would be necessary to exclude Slp4-a from the basolateral membrane, and Rab3 may be important for subsequent Slp4-a transport to the lumen initiation membrane.

Next we analyzed the role of phospholipid binding for Slp4-a, using a phospholipid-uncoupled mutant (K>Q[16]). Slp4a-K>Q localized to subapical puncta of apical membranes (Figure S6G, Table 1), and conferred a partial rescue to morphogenesis (Figure 6B), suggesting that while the C2 domains can confer membrane localization, interaction of Slp4-a with additional factors (Rabs and SNARE complexes) may partially compensate for the lack of C2 domain function.

Slp4, in contrast to others Slps, binds to SNARE proteins by its linker domain[30,31]. To analyze SNARE-binding, we generated a chimeric construct of Slp4-a bearing Slp5 linker domain (Slp4-5-4) that was unable to bind Syntaxin3 (Stx3) (Figure 6D). Slp4-5-4 showed a subapical and basolateral localization, and failed to rescue lumen formation upon endogenous Slp4-a KD (Figure 6E–F, S6I, Table 1), suggesting an important role for Stx3 binding to Slp4-a. Next, we mapped the Stx3 binding domain of Slp4-a, and identified aa 305–354 to be essential for Stx3 binding (Figure S6H). Consistently, expression of a construct lacking aa 305–354 of Slp4-a (GFP-Slp4-Δ305–354) also failed to localize to the

apical plasma membrane and to rescue lumen formation upon endogenous Slp4-a KD (Figure 6E, S6J, Table 1).

Stx3 functions as a critical apical SNARE[32]. In cysts, GFP-Stx3a colocalized with Slp4-a at the nascent luminal membrane (Figure 6G). Notably, Stx3 KD resulted in disruption of lumen formation and the redistribution of a pool of GFP-Slp4 to the basolateral membrane (Figure 6I–K), a similar localization observed upon removal of Stx-binding region of Slp4-a (Figure S6I–J). In contrast, Slp4-a KD did not disrupt the apical localization of Stx3 (Figure 6H). These data suggest that Stx3 association with Slp4-a, by interaction with the linker domain, directs recruitment of Slp4-a to apically destined vesicles, and initiation of *de novo* lumen formation.

Slp2-a regulates Slp4-a function to produce a single apical surface per cell

Our data thus far indicate that Slp2-a and Slp4-a function in distinct, non-redundant steps in Rab-dependent transport to form the lumen. We thus examined their localization during lumen formation. In early aggregates, Slp2-a localized mainly to cell-cell junctions, while Slp4-a colocalized with Podxl at the cell-ECM interface (Figure 7A, 16h, top panels, Figure S7C). As internalized Podxl transcytosed to the cell-cell contact, Slp4-a co-localized to these vesicles, whereas Slp2-a was mainly at the cell-cell junctions (Figure 7A, 20h, Figure S7C). Finally, Slp2-a/4-a co-localization was evident once lumens formed (Figure 7A, 24h, Figure S7C).

Next we tested if their activities were mutually dependent. KD of Slp2-a caused the scattered distribution of small Podxl-vesicles near the plasma membrane, with the latter pool only colocalizing with Slp4-a-GFP (Figure 7B), which had also been redistributed to the plasma membrane. In contrast, Slp4-a KD cysts presented with clusters of Podxl-vesicles (Figure 7C), but GFP-Slp2-a localized normally to cell-cell contacts, suggesting that Slp2-a localization and function is independent of, or upstream to, Slp4-a. Furthermore, overexpression of GFP-Slp2-a forced endogenous Rab27a and Slp4a mis-recruitment to cell-cell contacts at early time points (Figure 7D), while the converse effect of GFP-Rab27a on Slp2-a was not observed (not shown). These results suggest that Slp2-a functions to regulate the positioning of Rab27 vesicles upstream of Slp4-a-mediated vesicle docking, thus controlling the position of the apical membrane and subsequent lumen.

To test this hypothesis, we silenced Slp2-a and Slp4-a alone or together (Figure 7E–G). Strikingly, we observed that while Slp4-a KD induced accumulation of Podxl vesicles close to the membrane (Figure 7E, middle panels), Slp2-a KD cysts possessed some cells simultaneously developing more than one apical membrane (Figure 7E, top panels, quantification 7G). And while dual KD cysts presented a mixture of both phenotypes (Figure 7E, bottom panels), they perturbed single lumen formation to a level resembling that of Slp4-a KD alone, supporting the notion that Slp4-a functions downstream of Slp2-a (Figure 7F). Although cysts with multiple lumens have been observed previously upon KD of trafficking proteins, the KD of Slp2-a is unique in that this is the first time, to our knowledge, that a cell can participate simultaneously in the generation of multiple luminal surfaces.

In summary, these results indicate that Slp2-a and Slp4-a form part of a core apical transport pathway that controls the positioning of Rab27a/b vesicles, and their subsequent Rab8/Rab3b/Stx3-dependent fusion with the apical plasma membrane, respectively, to form a single $PI(4,5)P_2$–enriched apical membrane and lumen during *de novo* apical domain biogenesis (Figure 7H).

DISCUSSION

One of the central, unsolved questions in epithelial biology concerns how apical-basolateral polarity is coordinated between neighboring cells to form a common, single luminal region. Making use of the fact that MDCK can undergo polarization into either in 2D or 3D, we have uncovered a gene set that specifically facilitates transition to 3D architecture. Interestingly, most of this gene set is downregulated in some glandular epithelial cancers, indicating potential clinical relevance in maintaining a polarized phenotype (Figure 1).

During the development of 3D polarity, apical membrane components are delivered to the site for lumen initiation, between neighboring cells to initiate a luminal space *de novo*[7,33]. What had remained unclear, though, was how this trafficking pathway was organized to direct vectorial transport to a singular position, thus allowing formation of a single apical membrane per cell. Here, we have identified a molecular pathway specifically upregulated during 3D morphogenesis that controls the formation and positioning of a single apical membrane per cell, through the complementary functions of Slp2-a and Slp4-a (Figure 7H). We demonstrate that Slp2-a controls the clustering of apically destined vesicles through the interaction with Rab27a/b and the association with $PI(4,5)P_2$ at the nascent apical membrane. Subsequently, Slp4-a acts as an effector of Rab27a/b, Rab8a/b and Rab3b on vesicles, to couple the vesicles to Stx3-mediated fusion events at the plasma membrane to create the lumen. Inhibition of this Slp2-a/4-a pathway perturbs this transport and ultimately causes formation of multiple apical membranes. These data support our model that Slp2-a and Slp4-a function in a spatiotemporal cascade to control vectorial apical transport (Figure 7H), a fact supported by their sequential transcriptional upregulation during cyst formation.

How may Slp2-a/4-a coordinate vectorial transport to a single lumen? In non-polarized cells, both Slp2-a and Slp4-a are considered as negative regulators of secretion, based on the fact that their overexpression attenuates secretory granule release[15–17,29,34]. Indeed, Slp4-a can interact with the closed (non-fusion-forming) confirmation of SNARE complexes[31]. To this end, transient overexpression of Slp2-a or Slp4-a in the presence of endogenous protein consistently reduced single-lumen-formation rates (Figure S7A–B), a trend which could be strongly reversed by expression of SHD-deleted Slp2-a/4-a, suggesting they may act as negative regulators of vesicle trafficking. However, Slp2-a/4-a are also clearly required for single lumen formation, thus suggesting a scenario where, rather than being considered as ‘negative’ or ‘positive’ regulators of exocytosis, Slp2-a/4-a act as molecular traffic wardens[34], controlling vectorial exocytosis through ensuring vesicles dock and fuse only at singular membrane domains to form a single, co-ordinated luminal space between neighboring cells.

In summary, we identified, for the first time, a transcriptionally regulated molecular pathway that controls the formation of a single apical surface per cell, addressing a major, long-term unanswered question in cell biology. Study of the responsible transcriptional machinery for lumenogenesis *in vivo* presents as a major future challenge to both cell and developmental biology.

METHODS

Two-step functional screening (Microarrays, RT-qPCR, RNAi, Oncomine)

A microarray-based differential expression analysis was conducted using the Affymetrix Canine Genome 2.0 platform. MDCK type II cells were grown in P100 dishes to form 2D monolayers or 3D cysts in Matrigel (at 10^5 cells/ml). Total RNA was isolated at 36h and purified using RNeasy (Qiagen) and 5 μg of RNA were submitted for microarray analysis (n=3) using Affymetryx platform at Parque Científico de Madrid (Cantoblanco, Madrid). The raw microarray data is deposited in NCBI GEO (Gene Expression Omnibus), accessible online by this number GSE32495. A LiMMA (FDR<0.05) analysis revealed a set of 1597 upregulated genes. The resulting data set was analyzed to select a maximum of 100 upregulated genes for qPCR validation. To further examine this selection, we used bioinformatic/bibliographic searches to analyze all 1597 upregulated genes for previously published references into function (RIFs), and Gene Ontology (GO) terms from human or mouse orthologues in NCBI databases. We selected genes with GO terms, or RIFs related to processes or mechanisms involved in changes in cell signaling, cell architecture and organ morphogenesis.

The list included a comprehensive list of GO terms related to cell polarity, membrane trafficking, cell-to-cell junction assembly and remodeling, cell cycle regulation, cytoskeleton regulation, and cell division, among others (complete list on demand). The second selection approach used STRING software (http://string-db.org/) to select genes interacting with pathways previously known to have a role in epithelial architecture or morphogenesis. From the resulting list, we selected 99 genes based on bibliographic research and designed specific primers to perform qPCR analysis validation of their overexpression pattern in 3D cyst formation.

After qPCR validation, a stealth®-siRNA library was custom designed to target 47 validated candidate genes (Invitrogen, USA). To perform the siRNA screening, MDCK cells were transfected with siRNA using Nucleofector-II (Lonza). Transfected cells were cultured for 2 days in 3D conditions and RNA extracts were analyzed by RT-PCR to check silencing efficiency (Table S2). Gene expression silencing was verified by RT-qPCR procedures (SYBR RT-PCR premix, Applied Biosystems), normalizing to GAPDH or HPRT expression. For functional analyses, transfected MDCK cells were grown for 3 days in Matrigel to form cysts, and lumen formation efficiency was quantified by confocal microscopy using the following markers to assess lumen formation: localization of the apical protein podocalyxin (Podxl), integrity of the actin cytoskeleton (F-actin; Phalloidin), adherens junctions (β-catenin), tight junctions (ZO-1), nuclei (DNA; DAPI).

Antibodies

Antibodies against α-tubulin (1:5000; T9026, Sigma-Aldrich), Rab27a (1:200; R4655, Sigma-Aldrich), GFP (1:500; a5455, Invitrogen), Rab8a (1:1000, 610845, BD Biosciences), mRFP/Cherry (1:250; PM005, MBL), Syntaxin-3 (1:200; Ab4113, Abcam), GST (1:5000; sc138), β-catenin (1:1000, sc7199), and Slp4-a (1:100; 34448) from Santa Cruz Biotechnology were commercial primary antibodies. The Slp2-a antibody was raised as a polyclonal serum against the Slp2-a SHD region and used as previously described[35]. Podxl antibody was a gift from the Ojakian laboratory (State University of New York Downstate Medical Center, Brooklyn, NY). ZO-1 (1:500; R4076) from DSHB. Peroxidase-conjugated donkey anti–mouse IgG and anti– rabbit IgG were used as secondary antibodies for Western blots (Jackson ImmunoResearch Laboratories, Inc.). Alexa Fluor–conjugated secondary antibodies (Alexa Fluor 405, 488, 555, or 647; Invitrogen) and TOPRO-3 or DAPI (for nuclear/DNA staining) were used in microscopy protocols.

Plasmids

Slp2-a and Slp4-a (full length and mutants) were cloned into either pEGFP-C1/C2 or pmCherry-C1 vector (Takara Bio Inc.). Human Slp4-a cDNA template was from Open Biosystems (Thermo Fisher). Plasmids kindly provided were: pEGFP-Slp1 (J. Peränen, U. Helsinki, Finland), pEGFP-STX3a (M. ter Beest, U. Chicago, IL), pENTR-Rab3a/b/c/d (Bruno Goud, Institut Curie, Paris, France), pEGFP-Rab8a (María Montoya, CNIC, Madrid, Spain) and pEGFP-Rab27a/b (WT and DN) (John Hammer, NIH, USA). For bacterial expression of GST-tagged full length and mutant proteins, Slp2-a and Slp4-a were cloned into pGEX-4T1 vector (Promega) or pDEST15 (Invitrogen). Slp2-a (V18A, E11A/R32A[16]), and Slp4-a (V21A, W118S, I18A, K>Q[17,29]) mutants were generated using Quickchange XL (Stratagene). To disrupt C2 domain-lipid interactions in Slp4-a (C2AB K>Q; K410Q, K412Q, K416Q, K564Q, K566Q, K571Q), three of four Lysine residues of the PIP-binding consensus motifs present in Synaptotagmin and Synaptotagmin-like familiy C2 domains [K(K/R)KTXXK(K/R)] were mutated to Glutamine in both C2 domains, as reported for Slp2-a[16]. To disrupt Stx interactions in Slp4-a, the linker domain of Slp4-a was substituted for the linker domain of Slp5 (GFP-Slp4-5-4a) by subcloning the chimeric SHD_{Slp4}-$linker_{Slp5}$ fragment from a previously reported Slp4-5-4b construct[30] into a GFP-Slp4-C2AB plasmid. T7-tagged Slp4-a, Slp4-5-4a, and Slp4-a linker were used for in vitro syntaxin-3 binding experiments as previously reported[31,30]. The Slp4-a construct lacking the Stx3-interacting aminoacids of the linker domain (Δ305–354) was cloned into pEGFP-C1. All constructs were verified by sequencing.

Cells and 3D culture

T23-MDCKII and MDCKII cells were grown as described previously[9]. MDCK cells stably expressing GFP-Slp2-a (Full-length and mutants), Cherry-Slp2-a, GFP-Rab27a, GFP-Rab8a, and PLCδ-PH-GFP were made by cotransfection with the blasticidin-resistant gene and selected for 10 days with 0.5 μg/ml blasticidin. MDCK cells stably expressing GFP-Slp1, Stx3-GFP or GFP-Slp4-a (Full-length and mutants) were selected for 10 days using G418 (0.5 mg/ml). Cysts and transwells cultures were prepared as described before[36]

Microscopy

Immunofluorescence of cysts was as previously described[9, 36]. Per condition, >100 cysts/experiment were analyzed. For early time points, cysts were grown up to 24h and two/three-cell stage cysts were clasified based on Podxl and β-catenin localization either as “formed preapical-patch” or “presence of internal vesicles”.

RNAi

RNAi sequences and qPCR primers are listed in Supplementary Table 3. Briefly, 25 nucleotide stealth siRNA duplexes targeting mRNA sequences of canine Slp2-a were purchased from Invitrogen. Sequences were submitted to BLAST search to ensure targeting specificity. For siRNA transfection, MDCK cells were trypsinized and then nucleofected (Lonza) with siRNA duplexes or scrambled siRNA. After 24-h incubation, cells were resuspended and plated in 12-well plates and in coverglass chambers coated with matrigel to grow cysts. Total cell lysates from 3D cultures were analyzed by Western blotting or quantitative real-time PCR (Q-PCR) to confirm siRNA efficiency.

Stable RNAi was achieved by viral shRNA, essentially as previously described[7]. In all instances KD was verified by western blot or qRT-PCR procedures (Brilliant-II SYBR Green Kit, Agilent, Santa Clara, CA), normalizing to GAPDH expression. RNAi and qRT-PCR primers are presented in Supplementary Table 3. STX3 shRNA is as described[37]. SLP1 and SLP4-a shRNA lentiviruses were constructed in pLKO.1-puro according to the Addgene pLKO.1 protocol (www.addgene.org) using iRNAi (www.mekentosj.com), and target sequences were based on an (AA)N19 algorithm. RNAi sequences were submitted to BLAST (NCBI) to verify target specificity, with SLP4-a sequences targeting common regions to Slp4a and Slp4b transcripts. GFP-tagged human SLP4, which is not targeted by anti-canine shRNA, was used for Slp4-a KD and rescue experiments.

Virus production and transduction

Lentivirus production was performed essentially as previously described[7]. For lentivirus transductions, subconfluent MDCK cultures, 1–4 h after plating, were infected with virus-containing supernatants for 12–16 h at 37°C. Viral supernatants were then diluted 1:1 with growth medium, cultured for a further 48 h. Transduced cells were selected by passage into appropriate antibiotic-containing medium. Puromycin (5 μg/ml), and blasticidin (12.5 μg/ml) were used.

Statistics

Single lumen formation was quantified as described[7]. The percentage of cysts with a single lumen was determined, and normalized to control cysts as 100%. Values are mean ± SD from ≥3 replicate experiments, with n ≥100 cysts/replicate. For qRT-PCR experiments, percentage remaining mRNA in each KD condition was normalized to HPRT level, and represented as a percentage of control (scramble shRNA) mRNA levels. Significance was calculated using a paired, two-tailed Student’s t-test. *$p < 0.05$, ** < 0.001.

Rab-GTPase pull-down

Rab GTPase-Slp protein pulldowns were performed using HEK293T cells overexpressing GFP-tagged Rab proteins, and GST-tagged Slp proteins. HEK293T expressing GFP-tagged Rab proteins were lysed in 0.1% SDS, 1% Triton X-100, 0.5 mM DTT, and 1× TBS buffer with protease inhibitor cocktail and sodium orthovanadate. Cell debris and nuclei were removed by centrifugation at 14,000 × g for 2 min at 4°C, and lysates were precleared and incubated in rotation with 100 ng relevant GST protein–loaded beads (GE Amersham) for 30 min, using GST alone as control, in presence of non-hydrolizable GTP analog (Sigma). Beads were centrifuged and washed five times, dried using aspiration, and resuspended in 40 μl Laemmli buffer before Western blot analysis.

Co-Immunoprecipitation assays

Co-immunoprecipitation assays in COS-7 cells were performed essentially as described previously[30,31]. In brief, pEF-Flag-Stx3, pEF-Flag-Munc18-2, pEF-T7-Slp454 (a linker domain-swapping construct between Slp4a and Slp5[30] or pEF-T7-Slp4a linker deletion constructs (i.e., Linker, amino acids (AA) 144–354; F1, AA144–240; F2, AA215–304; and F3, AA272–354) were transfected into COS7 cells by using Lipofectamine 2000 (Invitrogen) according to the manufacturer's instructions. Cells were harvested 48 h after transfection and homogenized in a homogenization buffer[30,31]. After removal of insoluble materials by centrifugation, cell lysates were obtained. The associations between T7-tagged proteins and FLAG-tagged Stx3/Munc18-2 in the cell lysates were evaluated by immunoprecipitation using anti-T7 tag antibody-conjugated agarose beads (Merck Biosciences) as described previously[38]. Immunoreactive bands were visualized with horseradish peroxidase (HRP)-conjugated anti-T7 tag antibody (1:10,000 dilution; Novagen, 69522-4) and HRP-conjugated anti-FLAG tag M2 antibody (1:10,000 dilution; Sigma-Aldrich, A8592) and detected by enhanced chemiluminescence (ECL; GE Healthcare). For Rab-GTPase co-immunoprecipitation assay was performed as previously described[22].

PIP-strip and Lipid bead protein binding assays

A solution of 1 μg/ml of purified protein (GST, GST-Slp2-a, GST-Slp4-a) was incubated with PIP-strip membranes according to the instructions of the manufacturer (Echelon Bioscience). Lipid beads (Echelon) prepared with different phosphoinositides or phosphatidylserine were incubated with 2 μg of purified GST-C2A or GST-C2B from Slp2-a or Slp4-a, washed five times, dried and resuspended in 100 μl sample buffer before Western blot analysis. ECL blotting of membranes was developed by immunostaining with an anti-GST antibody (Sigma-Aldrich) and HRP-conjugated donkey anti-mouse IgG (Jackson Immunoresearch).

Supplementary Material

Refer to Web version on PubMed Central for supplementary material.

ACKNOWLEDGEMENTS

We thank Carmen M. Ruiz-Jarabo for comments on the manuscript, and members of Martin-Belmonte lab for discussion. We thank M. ter Beest J. Peränen, and K. Simons for generous gifts of reagents, and the Mostov lab for

kind assistance. Work supported by grants from Human Frontiers Science Program (HFSP-CDA 00011/2009), Marie Curie (IRG-209382), MICINN (BFU2008-01916), (BFU2011-22622) and CONSOLIDER (CSD2009-00016) to FM-B; by NIH R01DK074398, R01AI25144 and R01DK91530 to KM, and The March of Dimes Basil O'Connor Starter Research Award to PRB. AER-F is recipient of a JAE fellowship, from CSIC; MG-S is recipient of a FPI fellowship, from MICINN; and IB-R is recipient of an AECC fellowship. An institutional Grant from Fundación Ramón Areces to CBMSO is also acknowledged.

REFERENCES

1. Mostov K, Su T, ter Beest M. Polarized epithelial membrane traffic: conservation and plasticity. Nat Cell Biol. 2003; 5:287–293. [PubMed: 12669082]
2. Rodriguez-Boulan E, Musch A, Le Bivic A. Epithelial trafficking: new routes to familiar places. Curr Opin Cell Biol. 2004; 16:436–442. [PubMed: 15261677]
3. Bryant DM, Mostov KE. From cells to organs: building polarized tissue. Nat Rev Mol Cell Biol. 2008; 9:887–901. [PubMed: 18946477]
4. Datta A, Bryant DM, Mostov KE. Molecular regulation of lumen morphogenesis. Curr Biol. 2011; 21:R126–R136. [PubMed: 21300279]
5. Lubarsky B, Krasnow MA. Tube morphogenesis: making and shaping biological tubes. Cell. 2003; 112:19–28. [PubMed: 12526790]
6. Roland JT, et al. Rab GTPase-Myo5B complexes control membrane recycling and epithelial polarization. Proc Natl Acad Sci U S A. 2011; 108:2789–2794. [PubMed: 21282656]
7. Bryant DM, et al. A molecular network for de novo generation of the apical surface and lumen. Nat Cell Biol. 2010; 12:1035–1045. [PubMed: 20890297]
8. Gassama-Diagne A, et al. Phosphatidylinositol-3,4,5-trisphosphate regulates the formation of the basolateral plasma membrane in epithelial cells. Nat Cell Biol. 2006; 8:963–970. [PubMed: 16921364]
9. Martin-Belmonte F, et al. PTEN-mediated apical segregation of phosphoinositides controls epithelial morphogenesis through Cdc42. Cell. 2007; 128:383–397. [PubMed: 17254974]
10. Kuroda TS, Fukuda M, Ariga H, Mikoshiba K. The Slp homology domain of synaptotagmin-like proteins 1–4 and Slac2 functions as a novel Rab27A binding domain. J Biol Chem. 2002; 277:9212–9218. [PubMed: 11773082]
11. Ishii N, et al. A case of recurrent gall bladder cancer responding to chemotherapy with gemcitabine after endoscopic metallic biliary stent implantation. Gan To Kagaku Ryoho. 2008; 35:1403–1405. [PubMed: 18701859]
12. Pilot F, Philippe JM, Lemmers C, Lecuit T. Spatial control of actin organization at adherens junctions by a synaptotagmin-like protein. Nature. 2006; 442:580–584. [PubMed: 16862128]
13. Bagnat M, Cheung ID, Mostov KE, Stainier DY. Genetic control of single lumen formation in the zebrafish gut. Nat Cell Biol. 2007; 9:954–960. [PubMed: 17632505]
14. Brady DC, Alan JK, Madigan JP, Fanning AS, Cox AD. The transforming Rho family GTPase Wrch-1 disrupts epithelial cell tight junctions and epithelial morphogenesis. Mol Cell Biol. 2009; 29:1035–1049. [PubMed: 19064640]
15. Holt O, et al. Slp1 and Slp2-a localize to the plasma membrane of CTL and contribute to secretion from the immunological synapse. Traffic. 2008; 9:446–457. [PubMed: 18266782]
16. Kuroda TS, Fukuda M. Rab27A-binding protein Slp2-a is required for peripheral melanosome distribution and elongated cell shape in melanocytes. Nature cell biology. 2004; 6:1195–1203. [PubMed: 15543135]
17. Yu M, et al. Exophilin4/Slp2-a targets glucagon granules to the plasma membrane through unique Ca2+-inhibitory phospholipid-binding activity of the C2A domain. Mol Biol Cell. 2007; 18:688–696. [PubMed: 17182843]
18. Sato T, et al. The Rab8 GTPase regulates apical protein localization in intestinal cells. Nature. 2007; 448:366–369. [PubMed: 17597763]
19. Fukuda M, Saegusa C, Mikoshiba K. Novel splicing isoforms of synaptotagmin-like proteins 2 and 3: identification of the Slp homology domain. Biochem Biophys Res Commun. 2001; 283:513–519. [PubMed: 11327731]

20. Chavas LM, et al. Elucidation of Rab27 recruitment by its effectors: structure of Rab27a bound to Exophilin4/Slp2-a. Structure. 2008; 16:1468–1477. [PubMed: 18940603]
21. Fukuda M. Versatile role of Rab27 in membrane trafficking: focus on the Rab27 effector families. J Biochem. 2005; 137:9–16. [PubMed: 15713878]
22. Bryant DM, et al. A molecular network for de novo generation of the apical surface and lumen. Nature cell biology. 2010; 12:1035–1045. [PubMed: 20890297]
23. Gassama-Diagne A, et al. Phosphatidylinositol-3,4,5-trisphosphate regulates the formation of the basolateral plasma membrane in epithelial cells. Nature cell biology. 2006; 8:963–970. [PubMed: 16921364]
24. Di Paolo G, De Camilli P. Phosphoinositides in cell regulation and membrane dynamics. Nature. 2006; 7112:651–657. [PubMed: 17035995]
25. Zoncu R, et al. Loss of endocytic clathrin-coated pits upon acute depletion of phosphatidylinositol 4,5-bisphosphate. Proceedings of the National Academy of Sciences of the United States of America. 2007; 104:3793–3798. [PubMed: 17360432]
26. Bolasco G, et al. Loss of Rab27 function results in abnormal lung epithelium structure in mice. Am J Physiol Cell Physiol. 2011; 300:466–476.
27. van IJzendoorn SC, Tuvim MJ, Weimbs T, Dickey BF, Mostov KE. Direct interaction between Rab3b and the polymeric immunoglobulin receptor controls ligand-stimulated transcytosis in epithelial cells. Dev Cell. 2002; 2:219–228. [PubMed: 11832247]
28. Schlülter OM, Schmitz F, Jahn R, Rosenmund C, Südhof TC. A complete genetic analysis of neuronal Rab3 function. J. Neurosci. 2004; 24:6629–6637. [PubMed: 15269275]
29. Fukuda M, Kanno E, Saegusa C, Ogata Y, Kuroda TS. Slp4-a/granuphilin-a regulates dense-core vesicle exocytosis in PC12 cells. J Biol Chem. 2002; 277:39673–39678. [PubMed: 12176990]
30. Tsuboi T, Fukuda M. The Slp4-a linker domain controls exocytosis through interaction with Munc18-1.syntaxin-1a complex. Mol Biol Cell. 2006; 17:2101–2112. [PubMed: 16481396]
31. Fukuda M, Imai A, Nashida T, Shimomura H. Slp4-a/granuphilin-a interacts with syntaxin-2/3 in a Munc18-2-dependent manner. J Biol Chem. 2005; 280:39175–39184. [PubMed: 16186111]
32. Low SH, et al. The SNARE machinery is involved in apical plasma membrane trafficking in MDCK cells. The Journal of cell biology. 1998; 141:1503–1513. [PubMed: 9647644]
33. Schluter MA, et al. Trafficking of Crumbs3 during cytokinesis is crucial for lumen formation. Mol Biol Cell. 2009; 20:4652–4663. [PubMed: 19776356]
34. Gomi H, Mizutani S, Kasai K, Itohara S, Izumi T. Granuphilin molecularly docks insulin granules to the fusion machinery. The Journal of cell biology. 2005; 171:99–109. [PubMed: 16216924]
35. Imai A, Yoshie S, Nashida T, Shimomura H, Fukuda M. The small GTPase Rab27B regulates amylase release from rat parotid acinar cells. J Cell Sci. 2004; 117:1945–1953. [PubMed: 15039459]
36. Rodriguez-Fraticelli AE, et al. The Cdc42 GEF Intersectin 2 controls mitotic spindle orientation to form the lumen during epithelial morphogenesis. J Cell Biol. 2010; 189:725–738. [PubMed: 20479469]
37. Schuck S, Manninen A, Honsho M, Fullekrug J, Simons K. Generation of single and double knockdowns in polarized epithelial cells by retrovirus-mediated RNA interference. Proceedings of the National Academy of Sciences of the United States of America. 2004; 101:4912–4917. [PubMed: 15051873]
38. Fukuda M, Kanno E. Analysis of the role of Rab27 effector Slp4-a/Granuphilin-a in dense-core vesicle exocytosis. Methods Enzymol. 2005; 403:445–457. [PubMed: 16473610]

HIGHLIGHTS

- A functional screen reveals 14 previously undescribed regulators of lumen formation
- Slp2-a controls positioning of Rab27a/b-postive vesicles during lumen initiation
- Slp4-a controls fusion of apically destined vesicles with the plasma membrane to initiate the lumen
- Slp2-a/Slp4-a cooperate to ensure only a single lumen forms

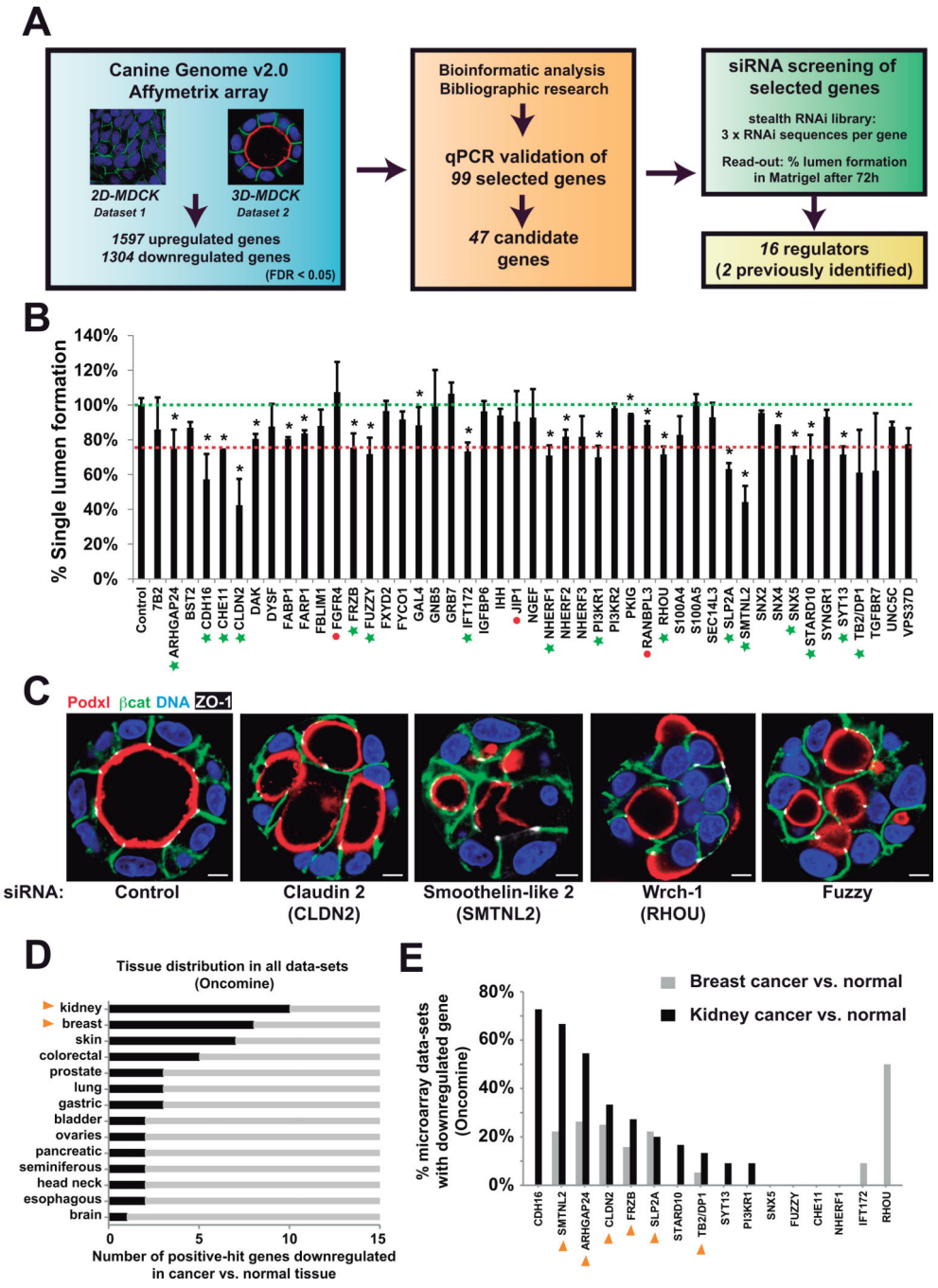

Figure 1. A screen for regulators of 3D epithelial polarization

(A) Experimental design for function screen of regulators of 3D epithelial polarity. MDCK cells cultured for 36h in 2D or 3D (n=3) and control (2D) and experimental (3D) samples were analyzed using the Affymetrix Canine Genome 2.0 platform. Significant data was determined by FDR-LIMMA (FDR<0.05). A set of significantly upregulated (>2-fold) genes was pooled with other genes of interest and then gene overexpression was validated by RT-qPCR. Bioinformatic pathway analyses revealed that some genes were connected in common functional pathways. A final set of 47 candidates were selected for stealth® siRNA

design. MDCK cells were transfected with siRNAs individually or in pools and cultured to grow cysts. Silencing efficiency of the siRNA was determined by RT-qPCR. Then, cells were fixed and stained with Podxl, β-catenin and nuclei to quantify normal lumen formation. The RNAi screening finally resulted in 16 positive hits (see Methods)

(B) RNAi screening for polarization regulation. Lumen formation efficiency was quantified for each of the listed 47 siRNA treatment. Green dotted line, 'normal' levels as found in control; red dotted line, the threshold considered for the definition of a positive hit (Lumen formation < 75 % of control; $p<0.05$,). Green stars, positive hits. Red dots, KDs where efficiency was below 60%. Asterisks represent statistical significance ($p<0.05$). n = 3; error bars represent SD.

(C) Examples of phenotypes induced by RNAi in the screen. 72h MDCK cysts transfected with siRNA from 4 positive candidates (SMTNL2, CLDN2, RHOU, FUZ) and stained with apical marker Podxl (red), basolateral marker β-catenin (green), tight junction marker ZO-1 (white), and nuclei (blue). Bar, 5μm.

(D) Epithelial cancers with downregulated 3D polarity gene set. The expression levels of the candidate-gene-set in all cancer vs. normal expression datasets were analyzed using Oncomine (www.oncomine.org). The graph shows the number of downregulated genes per type of indicated epithelial cancers ($p<0.05$, n varies in each tissue).

(E) Frequency of gene downregulation in breast and kidney cancer data-sets. The graph indicates the % of data-sets with downregulated candidate gene in breast and kidney cancer vs. normal tissue microarray data-sets (Oncomine, $p<0.05$). Yellow arrowheads denote genes downregulated in both, breast and kidney cancer.

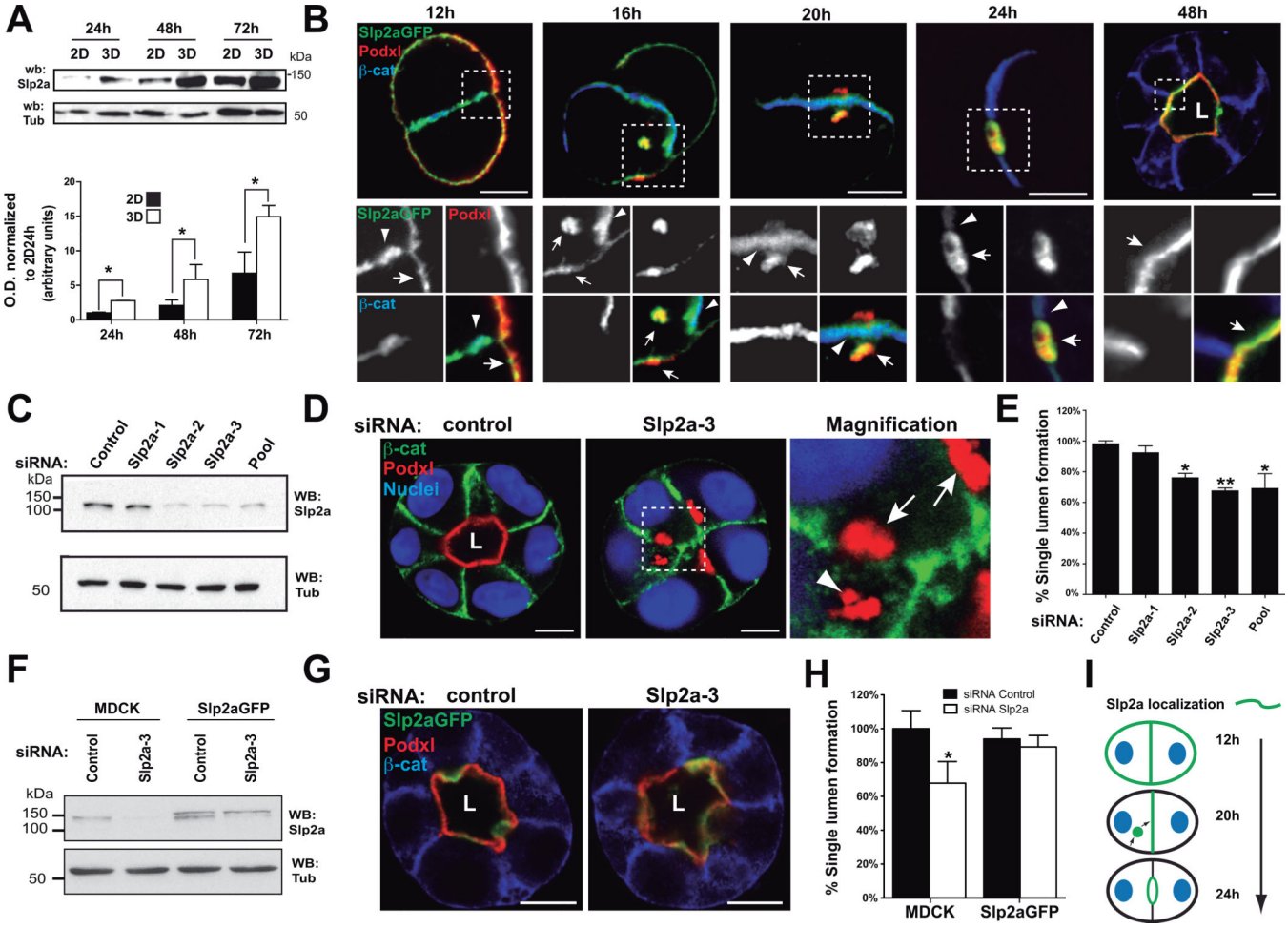

Figure 2. Slp2-a is required for epithelial morphogenesis

(A) Western-blot showing induction of Slp2-a in MDCK cells growing in 2D and 3D at different time points (24 to 72h). Bottom panel shows expression quantified by densitometry (n=4).

(B) Localization of GFP-Slp2-a during lumen formation. MDCK cells stably expressing GFP-Slp2-a were grown in 3D and fixed at different time points. Cysts were stained with Podxl (red) and β-catenin (blue). Arrows indicate localization to apical plasma membrane; arrowheads indicate localization to cell-cell junctions; L, lumen. Bar, 5μm.

(C) Downregulation of Slp2-a by siRNA. MDCK cells were transfected with three different siRNA duplexes targeting canine Slp2-a, and siRNA efficiency was analyzed by Western-blot.

(D) Effect of Slp2-a siRNA–mediated silencing on lumen formation. Cells were transfected with a pool of siRNA to KD Slp2-a or siRNA control and plated to form cysts for 72 h. Markers are Podxl (red), β-catenin (green), and nuclei (blue). Arrows indicate apical membrane localization; arrowheads indicate localization to intracellular apical vesicles; L, lumen. Bar, 5μm.

(E) Quantification of cysts with normal lumens in cells transfected with control siRNA or Slp2-a siRNA. Normal lumen Slp2-a KD 62% of control, (n=5). Values are mean ± SD from five independent experiments (n=5; ≥100 cysts/experiments)
(F) KD of Slp2-a by siRNA in cells stably expressing GFP-Slp2-a. MDCK cells stably expressing GFPSlp2-a were transfected with Slp2-a or control siRNAs. Total lysates were blotted for Slp2-a using α-tubulin as a loading control.
(G) Rescue effect of GFP-Slp2-a in cells silenced for Slp2-a on lumen formation. Cells were stained for Podxl (red) and β-catenin (blue). L, lumen. Bar, 10μm.
(H) Quantification of cysts with normal lumens in cells expressing GFP-Slp2-a and transfected with control or Slp2-a siRNAs, n=3.
(I) Slp2a localization during lumen initiation. In early aggregates (12h), Slp2-a localizes to cell-cell junctions at sites of apical vesicle fusion. After the lumen is initiated (24h), Slp2-a remains polarized at the apical membrane. Green lines, Slp2-a; blue ovals, nuclei; black lines, basolateral membrane.
In all panels error bars represent SD, significance: *P < 0.05; **P < 0.005

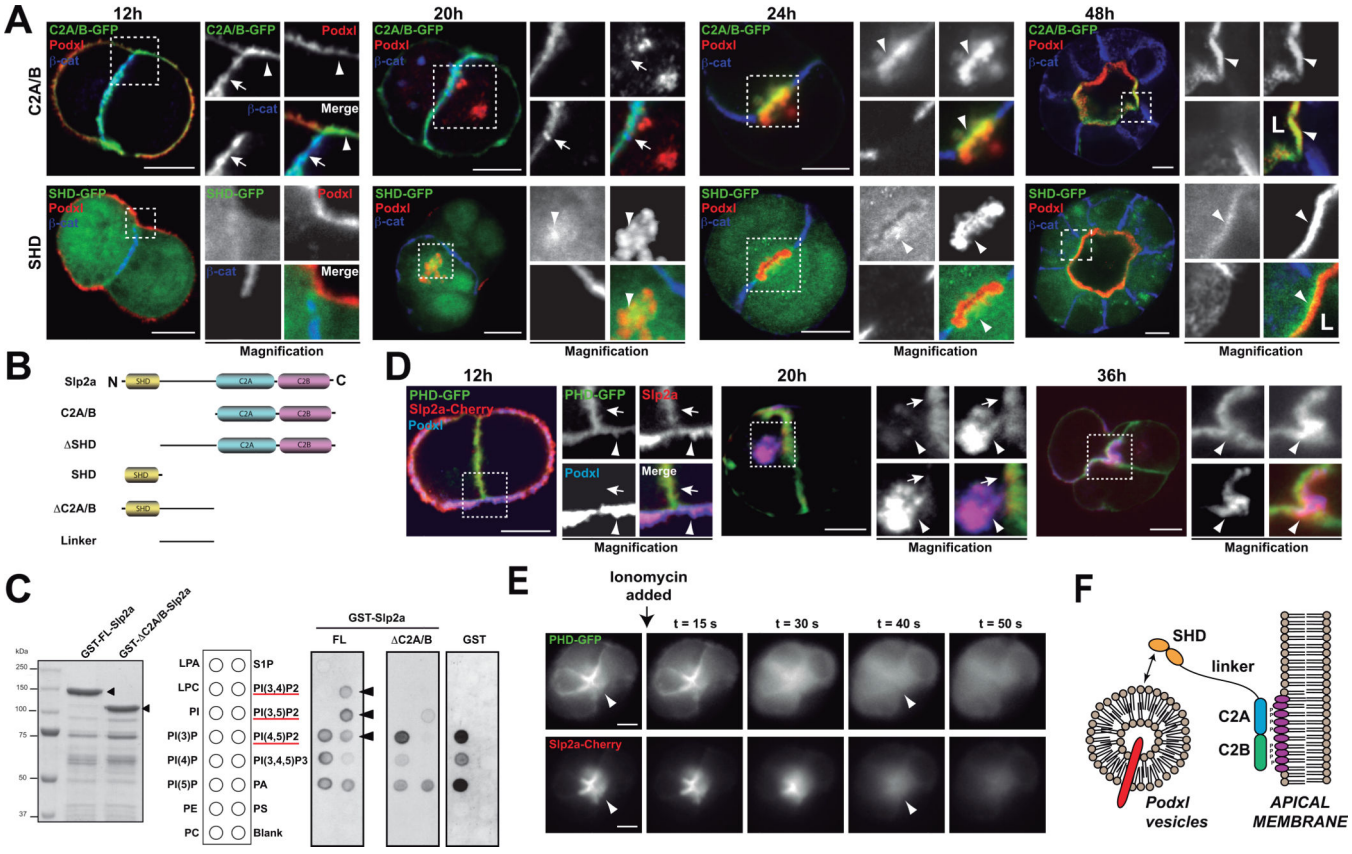

Figure 3. Slp2-a requires SHD and C2A/B domains for correct localization

(A) Localization of GFP-Slp2-a C2A/B, and SHD during lumen morphogenesis. MDCK cells stably expressing different GFP-Slp2-a constructs were grown in 3D to form cysts. Cysts were fixed at different time points (12, 20, 24 and 48h) and co-stained to detect Podxl (red) and β-catenin (blue). Arrowheads indicate apical membrane; arrows indicate localization to cell-cell junctions. Bar, 5μm.

(B) Scheme of Slp2-a constructs utilized. Different domains and truncated forms of Slp2-a were cloned for characterizing Slp2-a function.

(C) PIP-binding ability of Slp2-a. GST-tagged Full length Slp2-a (GST-FL) and ΔC2A/B (GST-ΔC2A/B), which should be unable to bind phospholipids, were expressed and purified in bacteria. PIP-strip membranes were incubated with 1 μg/ml concentration of GST (control), GST-FL or GST-ΔC2A/B and then membranes were blotted with anti-GST. A scheme of the PIP-strip membrane is shown. Arrowheads indicate specific PIP_2 binding. Red line highlights the phosphatidylinositol-bisphosphate species.

(D) Co-localization of Cherry-Slp2-a and $PI(4,5)P_2$ during early cyst formation. MDCK cells stably expressing Cherry-Slp2-a were transfected with the $PI(4,5)P_2$ probe (PHD-GFP) and grown in cysts. Cysts were fixed at different time points (12, 20, 36h) and co-stained to detect Podxl (blue). Arrowheads indicate apical membranes and arrows indicate cell-cell junction membrane localization. Bar, 5μm.

(E) Apical Slp2-a localization depends on $PI(4,5)P_2$. Cysts expressing PHD-GFP (top panels) and Cherry-Slp2-a (bottom panels), were treated with Ionomycin, which stimulates endogenous PLC activity to deplete membrane $PI(4,5)P_2$, and were analyzed by

videomicroscopy (0.1s exposure every 1s). Still images at different time points after Ionomycin addition are presented. Arrowheads indicate apical membrane localization. Bars, 10μm.

(F) Schematic of Slp2-a association with the apical plasma membrane. Slp2-a C2A/B domains bind PIP_2 and localize Slp2-a to the lumen initiation site and the apical membrane. SHD domain binds apical vesicles.

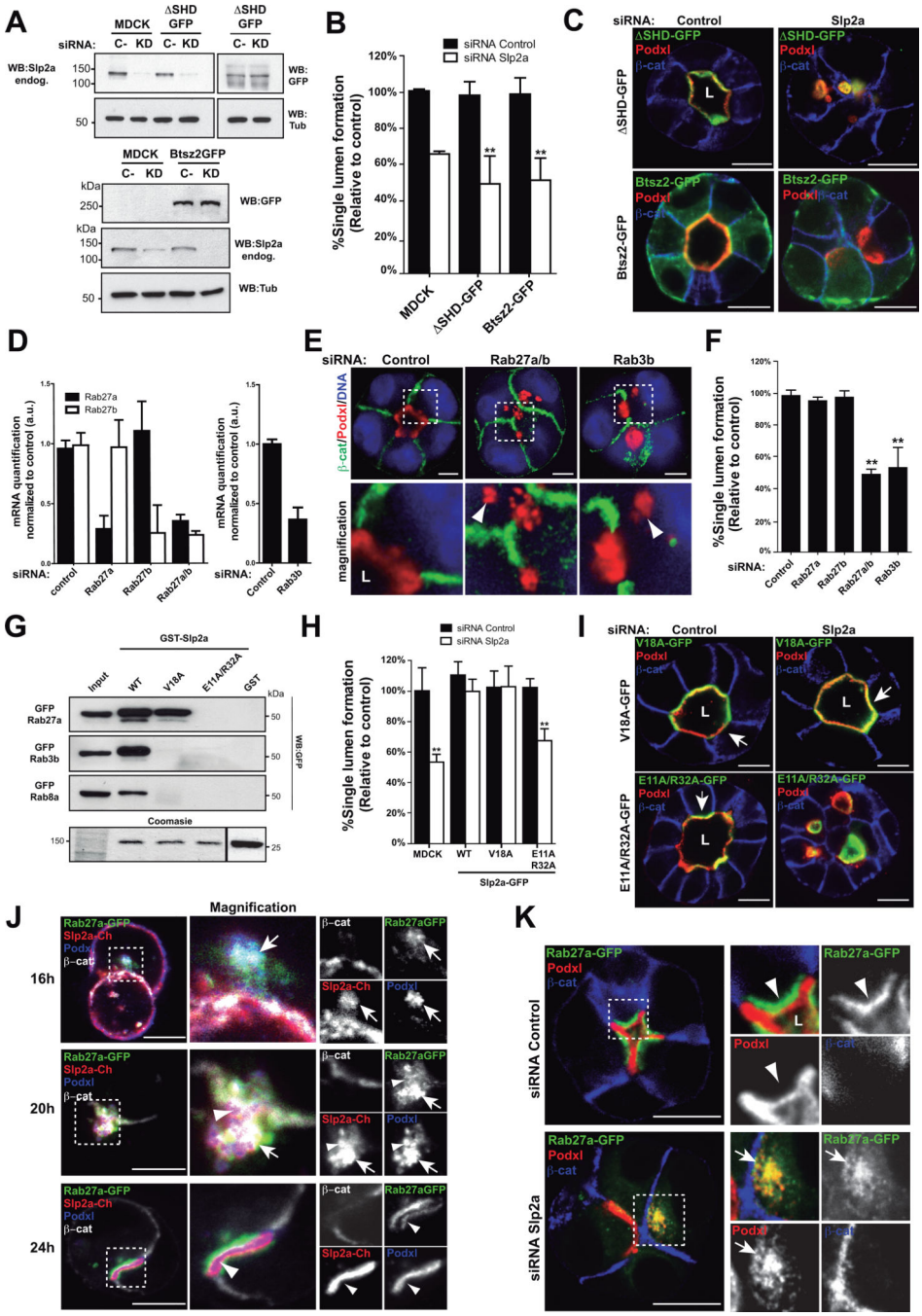

Figure 4. Slp2-a binds Rab27 to form the apical membrane

(A) KD of Slp2-a in cells stably expressing GFP-Slp2-a ΔSHD or Bitesize2-GFP (Btsz2) at 72h after siRNA transfection.

(B) Quantification of cysts with normal lumens in cells expressing GFP-ΔSHD or Bitesize2-GFP and transfected with siRNA to Slp2-a or control (n=3).

(C) Rescue effect of GFP-Slp2-a-ΔSHD and Bitesize2-GFP in cells KD for Slp2-a on lumen formation at 72h post siRNA transfection. Poxdl (red), β-catenin (blue). Note Bitesize2-GFP localization is not polarized on the plasma membrane of cysts.

(D) KD of Rab27a/b and Rab3b by siRNA. MDCK cells were transfected with different siRNA duplexes targeting canine Rab27a, Rab27b or Rab3b. After 72h RNA extracts were quantified by RT-qPCR, n=3.

(E) Effect of Rab27a/b or Rab3b KD in cyst formation. Cysts were fixed 48h after transfection. Silencing of Rab27a/b or Rab3b was sufficient to disrupt cyst formation and accumulate Podxl in vesicles (arrowheads). Podxl (red), β -catenin (green) or nuclei (blue)

(F) Quantification of cysts with normal lumens in cells transfected with siRNA targeting Rab27a, Rab27b, Rab27a/b or Rab3b (n=3).

(G) Rab-GTPase interaction with Slp2-a mutants V18A and E11A/R32A. GST (control) or GST-Slp2-a (WT, V18A, E11A/R32A) beads were used to pull-down fluorescent protein-tagged Rab3b, Rab8a or Rab27a from total cell lysates. Bottom lane, Coomasie staining of an independent polyacrylamide gel loaded with GST-Slp2-a constructs and a representative input.

(H) Quantification of normal cysts in cells expressing GFP-Slp2-a WT, V18A and E11A/R32A mutants transfected with siRNA against Slp2-a or control (n=3).

(I) Images of GFP-Slp2-a V18A and E11A/R32A cysts after Slp2-a KD. Cysts were fixed 48h after transfection. Poxdl (red), β-catenin (blue). Arrows indicate apical membrane.

(J) Colocalization of Rab27 and Slp2-a during cyst morphogenesis. MDCK cells stably expressing Cherry-Slp2-a and GFP-Rab27a were grown as cysts and fixed after 16, 20, or 24h. Podxl (blue), β-catenin (white).

(K) Effect of the downregulation of Slp2-a in GFP-Rab27a cells 36h after siRNA transfection. Arrowheads indicate Rab27a subapical localization. Arrows indicate colocalization of Podxl and Rab27a.

In all panels values are means ±SD of n independent experiments; Significance: *P < 0.05; **P < 0.005. L, lumen. Bar, 10μm.

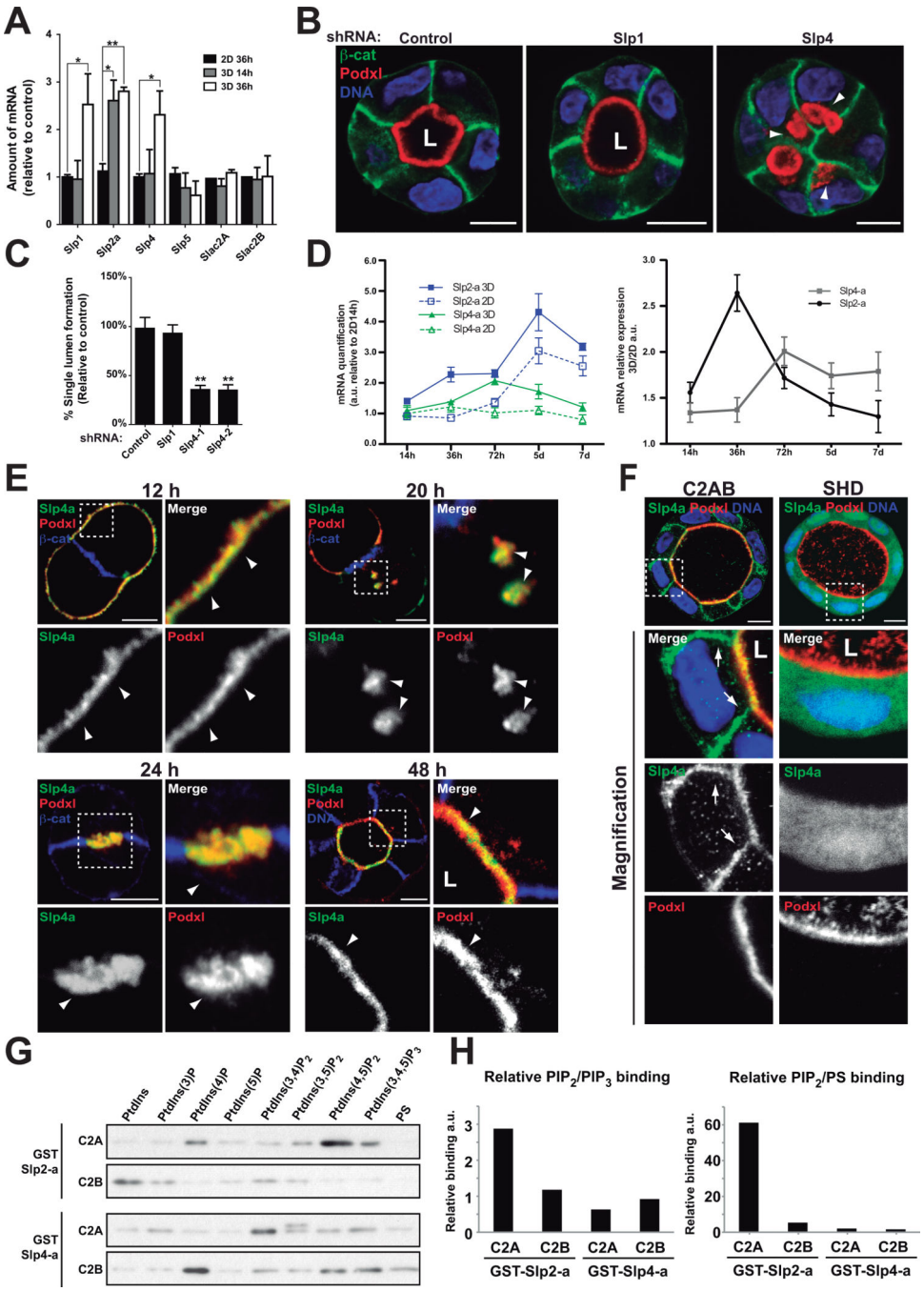

Figure 5. Slp4-a is required for epithelial morphogenesis

(A) Analysis of Slp and Slac2 expression in 2D vs 3D. Slp1, Slp2-a, Slp4-a, Slp5, Slac2A and Slac2B expression was evaluated at different time points (14h and 36h) by RT-qPCR in MDCK cells grown in 2D and 3D. Slp3, Slac2C and the related Rab27 effectors Noc2 and Rabphilin3 were not expressed in MDCK, n=4

(B) Effect of Slp4-a silencing on lumen formation. Cells stably expressing Slp4, Slp1 or scramble shRNA were plated to form cysts for 72 h. Cells were stained to detect Podxl (red), β-catenin (green), and nuclei (blue). Arrowheads indicate intracellular Podxl-vesicles.

(C) Quantification of cysts with normal lumens in cells expressing scramble, Slp1 or Slp4-a shRNA. (n=3)

(D) Quantification of Slp2-a and Slp4-a mRNA in cells grown on filters or in matrigel. MDCK cells were grown on filters to confluence (2D) or in matrigel (3D). mRNA expression was evaluated at different times by RT-qPCR. Data was normalized to 2D levels at 14h post-plating. Left panel represents Slp2-a (blue lines) and Slp4-a (green lines) mRNA expression patterns in 2D (continuous lines) or 3D (discontinuous lines). Right panel represents mRNA expression as 3D/2D coefficient at different time points, n=3

(E) Localization of GFP-Slp4-a in stably expressing cells during lumen formation. Cysts were stained with Podxl (red) and β-catenin (blue). Arrowheads indicate Slp4-a colocalization with Podxl.

(F) Localization of GFP-Slp4-a C2A/B and SHD during lumen morphogenesis. Cysts were fixed at 96h and co-stained to detect Podxl (red) and β -catenin (blue). Arrows indicate basolateral plasma membrane.

(G) Phospholipids binding ability of Slp2-a and Slp4-a C2 domains. Purified GST-tagged Slp2-a and Slp4-a C2A and C2B domains were incubated with beads covered with phosphoinositides or phosphatidylserine (PS).

(H) Quantification of relative binding of phosphoinositides and PS to Slp2-a and Slp4-a C2 domains. Graphics showing PIP_2/PIP_3 (left panels) or PS/PIP_2 binding ratio (right panels). Note Slp2-a C2A domain binds mainly to PIP_2 whereas other C2 domains show similar binding abilities to PIP_2, PIP_3 or PS.

In all panels values are means ±SD of n independent experiments; Significance: *P < 0.05; **P < 0.005. L, lumen. Bar, 10 μm.

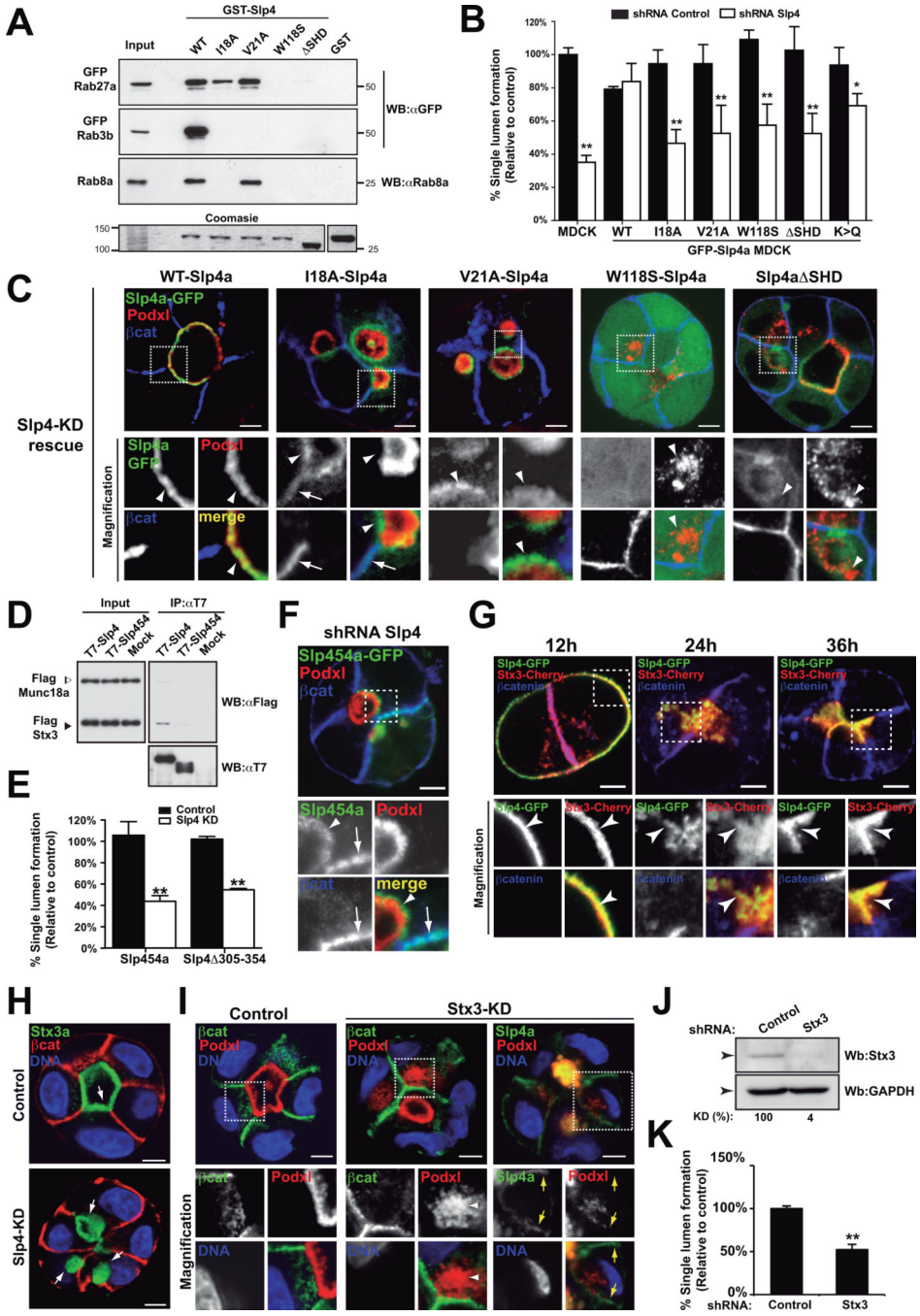

Figure 6. Slp4-a binding to PM, Rabs and Stx3 is required for apical membrane formation

(A) Rab-GTPase binding to Slp4-a mutants. Purified GST-tagged Slp4-a (WT, I18A, V21A, W118S and ΔSHD) or GST (control) proteins were used to pull-down fluorescent protein-tagged Rab3b, Rab8a or Rab27a from total cell lysates. Membranes were blotted with anti-GFP or anti-Rab8a. Bottom lane, coomasie staining of an independent polyacrylamide gel loaded with different GST-Slp4-a constructs and inputs.

(B) Quantification of cysts with normal lumens in GFP-Slp4-a (WT, ΔSHD, I18A, V21A, W118S and K>Q) cells expressing scramble or Slp4-a shRNA (n=3).

(C) Rescue effect of GFP-Slp4-a WT, Rab-binding defective mutants or membrane-binding defective Slp4-a (K>Q). MDCK cysts (72h) expressing GFP-Slp4-a WT, ΔSHD, I18A, V21A, W118S, or K>Q were KD for Slp4-a, and stained for Podxl (red) and β-catenin (blue). Co-localization with Podxl (arrowheads), β-catenin (arrows).
(D) Coimmunoprecipitation assay of Slp4a binding to Syntaxin3. T7-Slp4-a or T7-Slp4-5-4 beads were incubated with FLAG-Munc18-2 and FLAG-Stx3 lysates. FLAG-tagged proteins were detected with HRP-conjugated anti-FLAG. Input 1:10 of IP volume.
(E) Quantification of cysts with normal lumens in absence of Stx3-Slp4 interaction using cells expressing GFP-Slp4-5-4, or GFP-Slp4-a Δ305–354 and KD for Slp4-a (n=3).
(F) Localization of GFP-Slp4-5-4 in Slp4-a silenced cells. Podxl (red) and (blue). Arrowheads show vesicular localization; arrows basolateral membrane.
(G) Localization of Cherry-Stx3a and GFP-Slp4-a during cyst development. Cherry-Stx3a co-localized with GFP-Slp4-a at the periphery of early aggregates (arrowheads), intracellular vesicles, and cell-cell contacts. As lumens formed, Cherry-Stx3a concentrated at the nascent luminal membrane with GFP-Slp4-a (arrowheads). Nuclei (blue).
(H) Intracellular localization of GFP-Stx3a (arrows) in Slp4-a KD cysts (72h). β-catenin (red) and nuclei (blue).
(I) GFP-Slp4-a localization in 48h cysts KD for Stx3. Podxl (red), βcatenin (green) and nuclei (blue). Note Slp4-a basolateral mis-localization in Stx3 KD cysts (yellow-arrows). Arrowheads indicate Podxl-vesicles.
(J) Downregulation of Stx3a in MDCK cells stably expressing Stx3a shRNA. Total lysates were blotted for Stx3a and GAPDH (loading control).
(K) Quantification of the effect of Stx3 silencing in cyst formation (n=3).
In all panels values are means ±SD of n-independent experiments; Significance: *P < 0.05; **P < 0.005. Bar, 5 μm.

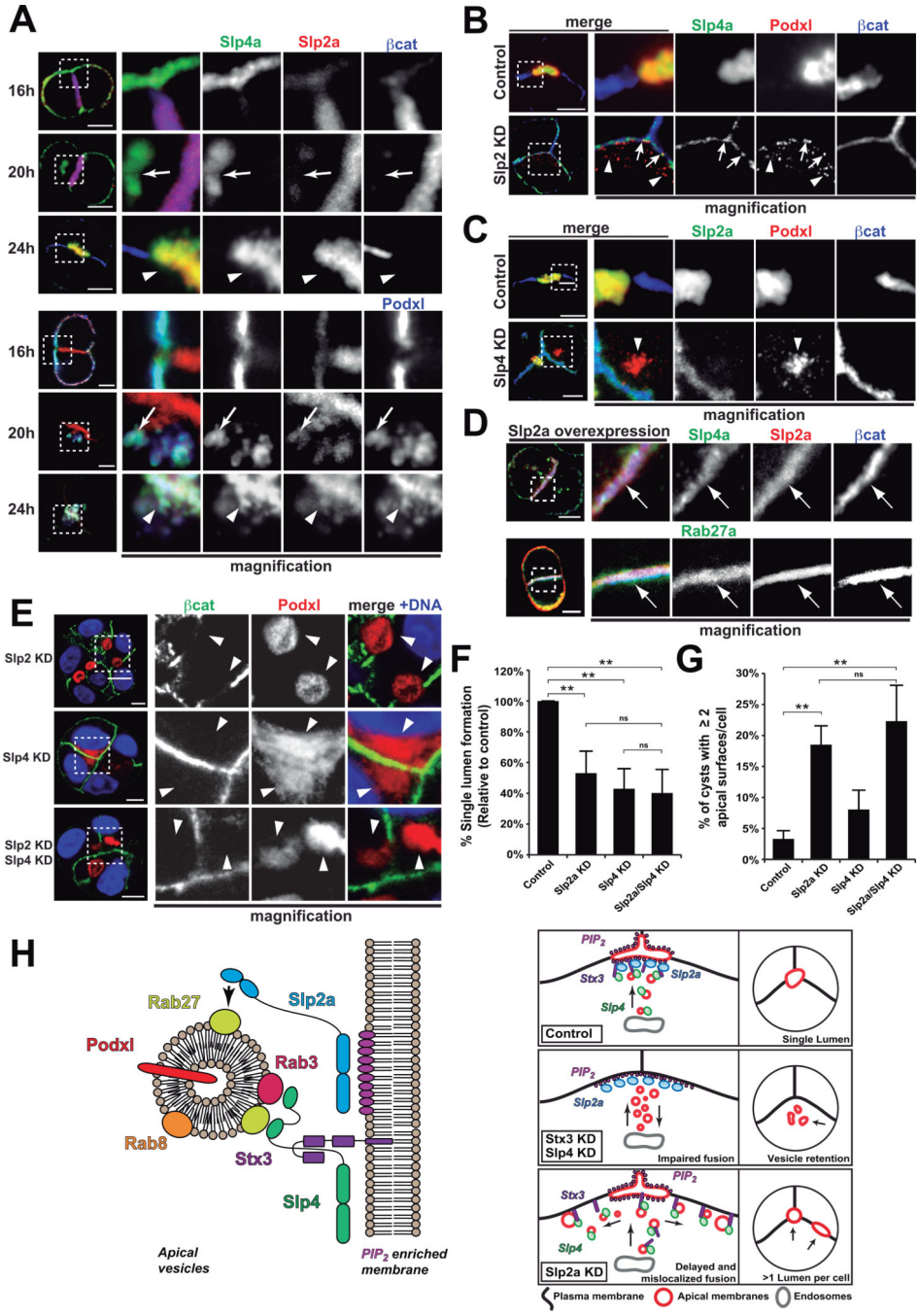

Figure 7. Slp2-a regulates Slp4-a targeting to determine single apical membrane formation

(A) Slp2-a and Slp4-a localization during lumen initiation. Cysts stably expressing GFP-Slp4-a and Cherry-Slp2-a were fixed after 16, 20 and 24h. Podxl (blue, bottom panels) and β-catenin (blue, top panels). Arrows indicate vesicular Slp4-a. Arrowheads indicate Slp2-a/Slp4-a colocalization at the nascent luminal membrane.

(B) Effect of Slp2-a KD on Slp4-a localization. Slp4-a localization becomes basolateral after Slp2-a KD and colocalizes partially with Podxl (red) in vesicles (arrows). Arrowheads indicate scattered Podxl vesicles.

(C) Effect of Slp4-a KD on Slp2-a localization. After Slp4-a KD, Slp2-a localization at cellular junctions is unaffected. Note accumulation of Podxl (red) in vesicles (arrowheads).
(D) Effect of Slp2-a overexpression on GFP-Slp4-a and GFP-Rab27 in 24h cysts. Slp4-a or Rab27a colocalized with Slp2-a and β-catenin(blue) at cellular junctions (arrows).
(E) Effect of double Slp2-a/Slp4-a KD on lumen formation. Cells KD for Slp4-a, Slp2-a, or Slp4-a/Slp2- for 48h were fixed and stained for nuclei (blue), Podxl (red) and β-catenin (green). Arrowheads indicate apical plasma membranes.
(F) Quantification of cysts with normal lumens in control, Slp2-a KD, Slp4-a KD, or Slp2-a/4-a double KD (n=3).
(G) Quantification of cysts presenting two or more apical surfaces per cell in control, Slp2-a KD, Slp4-a KD or Slp2-a/4-a double KDs (n=3).
In all panels values are mean ± SD from n independent experiments; Significance: ns, not-significant, **P < 0.005. Bars, 5 μm.
(H) Model of Slp2-a/4-a function in epithelial polarization. Left panel: Slp2-a targets Rab27-positive endosomes to the PIP_2-enriched membrane. Slp4-a binds to Rab3 and Stx3 to be delivered to the lumen initiation site in Rab27-positive vesicles. Because Slp4-a is delivered in Rab27-positive vesicles, its targeting depends on Slp2-a function. Therefore, Slp2-a directs localization of Slp4-a/Stx3-influenced vesicle tethering activity to single PIP_2-enriched initiation site, and thus a single lumen per cell. Right panel: When Slp4-a or Stx3 are perturbed, vesicles cannot be correctly tethered and apical vesicles accumulate. When Slp2-a is disrupted, vesicles are tethered ectopically to different positions of the plasma membrane, originating multiple apical domains in the same cell.

Table 1

Localization and function of Synaptotagmin-like proteins, and their mutants, in MDCK cyst formation. This table represents a qualitative summary of results regarding wild-type or mutant Slp protein localization (at different time points) and its ability to rescue the silencing of endogenous protein expression.

Protein	Construct	Cell localization			Mutant effect	Phenotype rescue
		early aggregate	lumen initiation	open lumen		
SLP2	Full-length	unpolarized PM	junctions PM	apical PM		YES
	SHD	vesicle/cytosolic	vesicle/cytosolic	vesicle/cytosolic		-
	ΔC2AB	vesicle/endosome	vesicle/endosome	subapical		-
	linker	cytosol	cytosol	cytosol		-
	ΔSHD	unpolarized PM	junctions PM	apical PM		NO
	C2AB	unpolarized PM	junctions PM	apical PM		-
	mut E11A/R32A	unpolarized PM	junctions PM	apical PM	no Rab binding	NO
	mut V18A	unpolarized PM	junctions PM	apical PM	no Rab3/8 binding	YES
SLP4	Full-length	apical PM	vesicles	apical PM		YES
	SHD	nuc/cytosol	nuc/cytosol	nuc/cytosol		-
	ΔC2AB	cytosol	cytosol	cytosol		-
	linker	cytosol	cytosol	cytosol		-
	ΔSHD	unpolarized PM	unpolarized PM	unpolarized PM		-
	C2AB	unpolarized PM	unpolarized PM	unpolarized PM		-
	mut I18A	unpolarized PM	vesicles/junctions PM	subapical/junctions PM	no Rab3/8 binding	NO
	mut V21A	vesicles	vesicles	subapical	no Rab3 binding	NO
	mut W118S	cytosol	cytosol	cytosol	no Rab binding	NO
	mut KQ	vesicles	vesicles	subapical	no lipid binding	Partial
	Slp454a	unpolarized PM	vesicles/PM	subapical/junctions PM	no SNARE binding	NO
	Δ305–354	unpolarized PM	vesicles/PM	junctions PM	no SNARE binding	NO